

ACCEPTED MANUSCRIPT

Deep level defects in 4H-SiC introduced by ion implantation: The role of single ion regime

To cite this article before publication: Zeljko Pastuovic *et al* 2017 *J. Phys.: Condens. Matter* in press <https://doi.org/10.1088/1361-648X/aa908c>

Manuscript version: Accepted Manuscript

Accepted Manuscript is “the version of the article accepted for publication including all changes made as a result of the peer review process, and which may also include the addition to the article by IOP Publishing of a header, an article ID, a cover sheet and/or an ‘Accepted Manuscript’ watermark, but excluding any other editing, typesetting or other changes made by IOP Publishing and/or its licensors”

This Accepted Manuscript is © 2017 IOP Publishing Ltd.

During the embargo period (the 12 month period from the publication of the Version of Record of this article), the Accepted Manuscript is fully protected by copyright and cannot be reused or reposted elsewhere.

As the Version of Record of this article is going to be / has been published on a subscription basis, this Accepted Manuscript is available for reuse under a CC BY-NC-ND 3.0 licence after the 12 month embargo period.

After the embargo period, everyone is permitted to use copy and redistribute this article for non-commercial purposes only, provided that they adhere to all the terms of the licence <https://creativecommons.org/licenses/by-nc-nd/3.0>

Although reasonable endeavours have been taken to obtain all necessary permissions from third parties to include their copyrighted content within this article, their full citation and copyright line may not be present in this Accepted Manuscript version. Before using any content from this article, please refer to the Version of Record on IOPscience once published for full citation and copyright details, as permissions will likely be required. All third party content is fully copyright protected, unless specifically stated otherwise in the figure caption in the Version of Record.

View the [article online](#) for updates and enhancements.

Deep level defects in 4H-SiC introduced by ion implantation: The role of single ion regime

Željko Pastuović, Rainer Siegele

Centre for Accelerator Science, Australian Nuclear Science and Technology Organisation, 1New Illawarra Rd, Lucas Heights NSW 2234, Australia

Ivana Capan, Tomislav Brodar

Division of Materials Physics, Rudjer Boskovic Institute, Bijenicka 54, 10 000 Zagreb, Croatia

Shin-ichiro Sato, Takeshi Ohshima

Takasaki Advanced Radiation Research Institute, National Institutes for Quantum and Radiological Science and Technology, 1233 Watanuki, Takasaki, Gunma 370-1292, Japan

We characterized intrinsic deep level defects created in ion collision cascades which were produced by patterned implantation of single accelerated 2.0 MeV He and 600 keV H ions into *n*-type 4H-SiC epitaxial layers using a fast-scanning reduced-rate ion microbeam. The initial Deep Level Transient Spectroscopy measurement performed on *as-grown* material in the temperature range 150-700 K revealed the presence of only two electron traps, $Z_{1/2}$ (0.64 eV) and $EH_{6/7}$ (1.84 eV) assigned to the two different charge state transitions of the isolated carbon vacancy, $V_C (=0)$ and $(0/+)$. C-V measurements of *as-implanted* samples revealed the increasing free carrier removal with larger ion fluence values, in particular at depth corresponding to a vicinity of the end of an ion range. The first DLTS measurement of *as-implanted* samples revealed formation of additional deep level defects labelled as ET1 (0.35 eV), ET2 (0.65 eV) and EH3 (1.06 eV) which were clearly distinguished from the presence of isolated carbon vacancies ($Z_{1/2}$ and $EH_{6/7}$ defects) in increased concentrations after implantations either by He or H ions. Repeated C-V measurements showed that a partial net free-carrier recovery occurred in *as-implanted* samples upon the low-temperature annealing following the first DLTS measurement. The second DLTS measurement revealed the almost complete removal of ET2 defect and the partial removal of EH3 defect, while the concentrations of $Z_{1/2}$ and $EH_{6/7}$ defects increased, due to the low temperature annealing up to 700 K accomplished during the first temperature scan. We concluded that the ET2 and EH3 defects: i) act as majority carrier removal traps, ii) exhibit a low thermal stability and iii) can be related to the simple point-like defects introduced by light ion implantation, namely interstitials and/or complex of interstitials and vacancies in both carbon and silicon sub-lattices.

2nd_revision_manuscript_JPCM-109666

I. INTRODUCTION

Single centres are mainly isolated point defects created during material growth or material engineering by the ion implantation and post-implantation thermal treatment. As a cumulative effect they can modify the electrical, mechanical and optical properties of the material as a whole. Defect engineering in semiconductors by means of patterned ion implantation in the *single-ion regime* can be used for deterministic formation of single centres in building blocks of optoelectronic devices offering a high potential for applications in information technology as well as quantum computing [1-4].

High quality (i.e. purity) crystalline silicon carbide material required for the development of novel devices can be grown at reasonable cost, which is lower to other comparable materials such as diamond [5]. The elimination of defects from SiC has facilitated its move to the forefront of the optoelectronics and power-electronics industries [6]. Nonetheless, because certain deep level defects have electronic states with sharp optical and spin transitions, they are increasingly recognized as a platform for quantum information and nanoscale sensing [7-15].

Deep level defects in the 4H polytype of SiC with a potential for the single charge or single photon sensing, manipulation or exchange include: 1) carbon-silicon divacancy (paired silicon and carbon vacancies) [7-9], 2) silicon vacancy [10], 3) carbon antisite-vacancy pair [12, 13], and nitrogen-vacancy centres [14, 15].

The most prominent defects in high-quality 4H-SiC epi-layers are so-called $Z_{1/2}$ and $EH_{6/7}$ defects [16, 17]. They have been shown to play a decisive role as recombination centers in 4H-SiC epi-layers. Recently, Son and co-workers assigned the $Z_{1/2}$ and $EH_{6/7}$ to different charge state transitions of the carbon vacancy (V_C), the former being related to a negative- U double acceptor state, $V_C(=0)$, while the latter was linked to a donor transition, $V_C(0/+)$ [18].

Schottky barrier diodes (SBDs) are among the most fundamental building blocks of electronic structures. We used the 4H-SiC epilayer to fabricate SBDs, and exposed them to a fast raster-scanning focused microbeam of reduced ion rate for the patterned implantation in the *single ion regime*. In this study we investigated the deep level defects created in collision cascades produced by the well separated (time and space scale) and individually recorded ion-projectiles being raster-implanted in tested 4H-SiC thin layers. The defects and their cumulative effects on electronic properties of high quality SBDs prepared on these high-resistivity *n*-type 4H-SiC

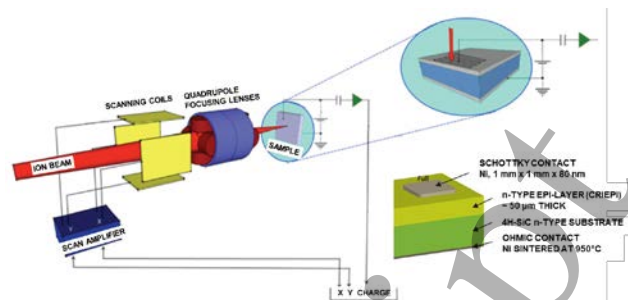


Figure 1. Schematics of the nuclear microprobe setup for patterned ion implantation of 4H-SiC Schottky barrier diode samples using a fast-scanning reduced-rate microbeam.

wafers were characterized by I-V, C-V and Deep Level Transient Spectroscopy (DLTS).

II. EXPERIMENTAL DETAILS

n-type silicon carbide SBDs were produced on nitrogen-doped (up to $5 \times 10^{14} \text{ cm}^{-3}$) epitaxial grown 4H-SiC single crystal layers approximately 50 μm thick [19]. The Schottky barrier was formed by evaporation of nickel through a metal mask with patterned square apertures of 1 mm \times 1 mm, while Ohmic contacts were formed by nickel sintering at 950 $^\circ\text{C}$ in Ar atmosphere on the back side of the silicon carbide substrate. The reverse negative bias was connected to the front Schottky contact, and the back Ohmic contact of prepared 4H-SiC SBD was grounded. Schematic of one tested SBD is shown in Figure 1. The quality of the prepared 4H-SiC SBDs was characterized by I-V and C-V measurements. Additional care was taken during final sample selection by performing the scanning Ion Beam Induced Charge (IBIC) microscopy [20, 21] in frontal mode to confirm a good uniformity of charge collection efficiency equal to 100% across the whole active surface of chosen SBDs.

The selected samples were pattern-implanted with either the 2 MeV He or 600 keV H ions at the ANSTO nuclear microprobe facility [22] in order to create deep level defects in 4H-SiC epitaxial layers. Schematic setup of the nuclear microprobe [23] for operation of focused ion microbeam in the *single ion regime*, with reduced particle rates in the 1-10 kHz range, is shown in Figure 1. An ion microbeam with a spot size (x, y) of $\sim 500 \text{ nm} \times 1000 \text{ nm}$ is rapidly raster-scanned (0.2 ms dwell time of a microbeam in each pixel) multiple times over a large area of the front Schottky metallization (1 mm \times 1 mm) divided in 512×512 pixels with the approximate pixel size of 2000 nm \times 2000 nm as shown in Figure 1. The IBIC technique was used for the direct single ion detection and counting the number of events. Approximately 1 or 2 ions were implanted in each pixel

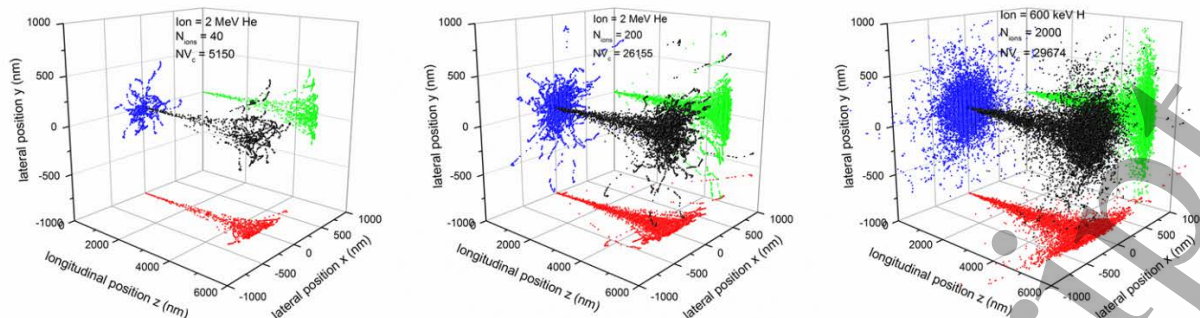


Figure 2 (a-c) 3D carbon vacancy distributions (black points) in a unit volume cell defined by the scanning pixel area (lateral coordinates) and the depth of ion range (longitudinal coordinate) following implantation of: (a) forty 2 MeV He, (b) two hundred 2 MeV He and (c) two thousand 600 keV H ions impinging at normal incidence into 4H-SiC epi-layer through front Ni contact. The lateral and two longitudinal projections of each vacancy position are designated by blue, red, and green points respectively. The ion, total number of implanted ions (N_{ions}) and total number of vacancies created in the unit cell (NV_c) of implanted samples #2, 3, and 4 are indicated in the plot legends.

before the microbeam was moved to the next pixel position. In such “single-ion” implantation conditions the interaction between primary defects created in subsequent or neighbouring cascades can be considered negligible, and created deep level defects are the product of interaction processes of primary displacements generated in each collision cascade well separated in space and time. Multiple repeated scans of a microbeam served just to create a sufficient concentration of deep level defects required for detection and analysis using the DLTS. The ion species and energies were chosen to obtain the lattice atom displacement density distribution within the depletion region of reversely biased partially damaged SBDs examined by the DLTS. The He ion fluence values used for these measurements correspond to the fluence range in which the charge collection efficiency in selectively implanted 4H-SiC epi-layers decreases linearly as a function of fluence, as demonstrated in our previous radiation hardness study of these epitaxial layers using the IBIC microscopy [24]. A negligible error of the calculated fluence values might be caused by a dead time of the data acquisition system. All implantations were performed at the room temperature and zero bias. Three samples were implanted and one pristine sample was used as a control. The samples were not thermally treated after implantations and before the first run of DLTS measurements. Details on prepared samples which were used for this study of deep level defects are provided in Table I.

Table I. Labelling and ion implantation conditions

Sample label	Ion	Rate (kHz) / Pixel dwell time (ms)	Energy (MeV)	Fluence (cm^{-2})	Number of ions per unit cell
#1		pristine			
#2	He	5 / 0.2	2.0	1×10^9	40
#3	He	5 / 0.2	2.0	5×10^9	200
#4	H	10 / 0.2	0.6	5×10^{10}	2000

III. RESULTS

A. Pre-implantation

Initial electrical measurements proved the excellent quality of prepared pristine SBD samples having a reverse current of the order of few pA and a terminal capacitance below 10 pF at -40 V (not shown here) [24]. The calculated free carrier concentration in pristine sample was $\sim 5 \times 10^{14} \text{ cm}^{-3}$ across the thickness of epitaxial layer. The calculated depletion depth in epitaxial layer was $\sim 4900 \text{ nm}$ for the pristine SBD biased at the reverse voltage of -10 V. Figures 2(a-c) show the spatial distribution of carbon vacancies, created in each unit volume cell defined by the scanning pixel area and the depth range in epitaxial layer, following implantation of a) forty He ions (sample #2), b) two hundred He ions (#3), and c) two thousand H ions (#4), at the same position (0,0,0) and at normal incident not aligned with crystal axis, simulated using the SRIM code [25]. In the real case of ion implantation using a microbeam with a finite spot size of $\sim 1000 \text{ nm}$, the entry point ($x, y, z = 0$) can be any with $-500 < (x, y) < 500$, and the incident angle to normal can be up to $\theta = 0.5^\circ$ (property of the unique microprobe design). The concentration of carbon vacancies gradually increases from the surface of epitaxial layer underneath the Ni contact layer and reaches a maximum close to the end of an ion range. It is worth noting that the lateral straggling of lighter H ions is larger than for He ions, and few isolated vacancies can be produced outside of the unit cell boundaries, i.e. in first-neighbour cells (Figure 2c). The silicon atom vacancy distributions (not shown here) exhibit the similar distributions, but their simulated concentrations are lower compared to the carbon vacancy concentrations due to differences in the displacement threshold energies for Si

2nd_revision_manuscript_JPCM-109666

(35 eV) and C atoms (22 eV) in 4H-SiC material [26]. It is expected that predominantly point-defects will be formed within the region of interest which can be tested with our DLTS apparatus (capable of supplying biases up to 10 V) due to these disordered regions rich with carbon or silicon vacancies and interstitials.

B. Free-charge carrier compensation

We observed the sharp decrease of capacitance for bias values which deplete the region of interest following the implantation of SBD samples (not shown here). Changes observed in $1/C^2$ vs. V characteristics (Figure 3) clearly indicate a decrease of the net free carrier concentration at depth corresponding to damaged regions rich in atomic displacements which are here represented with peaks in the carbon vacancy distributions. The net free-carrier concentration decrease is larger for samples with the higher concentration of produced atomic displacements #3 and #4. Therefore the free-carrier removal effect could be assigned to the cumulatively increasing concentration of ion-induced deep defects in the epi-layer (Figure 3). Such $1/C^2$ vs. V characteristics lead to the “anomalous” doping profiles (not shown here) reported by Kimerling *et al.* who described the great influence of deep defects on the free-carrier concentration profile estimated from the C-V measurements [27]. The influence is strongly pronounced for the acceptor defects with the inhomogeneous distribution, such as in our case of the ion implantation induced defects. The carrier removal is caused by the free electron trapping and the nitrogen compensation by created deep level defects. The obvious candidates for this effect are negatively charged point-like defects, vacancy or interstitial complexes.

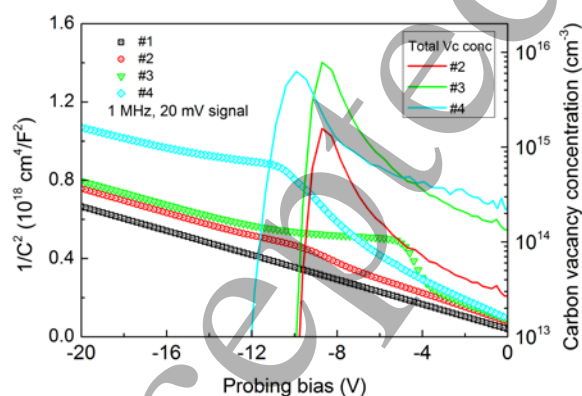


Figure 3. Results of 1 MHz C-V measurements for the pristine sample #1 (black squares), 2 MeV He implanted samples #2 (red circles), #3 (green up triangles), and 600 keV H implanted sample #4 (cyan rotated squares) are combined with simulated total carbon vacancy concentration distributions (lines) following implantation with 2 MeV He ions for fluence values of 1×10^9 cm⁻² (#2), 5×10^9 cm⁻² (#3), and with 600 keV H ions up to fluence value of 5×10^{10} cm⁻² (#4).

C. Defect analysis

Figure 4 shows DLTS spectrum of the pristine SBD sample (#1) for emission rate of 13.47 s⁻¹. Two peaks with their peak maxima at about 295 and 620 K were observed. They resemble defects known as $Z_{1/2}$ and $EH_{6/7}$ from the literature [16] and assigned to different charge state transitions of the carbon vacancy, ($=/0$) and ($0/+$), respectively.

In DLTS spectrum of the SBD sample implanted with 2.0 MeV He ions up to the lowest studied fluence value of 1×10^9 cm⁻² (#2) five peaks were observed with their peak maxima at about 190, 295, 340, 430 and 615 K (Figure 5). The emission rate was 13.47 s⁻¹. They are labelled as ET1, $Z_{1/2}$, ET2, EH3 and $EH_{6/7}$. The intensity of $Z_{1/2}$ and $EH_{6/7}$ peaks, already observed in the pristine sample (Figure 4), was increased upon the He ion implantation so as the asymmetric broadening. The calculated concentration of $Z_{1/2}$ defect in the pristine sample #1 (Figure 4) was $\sim 8 \times 10^{11}$ cm⁻³, while in the He implanted sample #2 (Figure 5) was increased to $\sim 3 \times 10^{12}$ cm⁻³. Recent DLTS and EPR studies made a clear confirmation that $Z_{1/2}$ and $EH_{6/7}$ are carbon vacancy defects [18]. V_C is the most dominant defect in 4H-SiC, often referred as a “lifetime-killer” due to the strong connection with the minority carrier lifetime [28], which is one of the crucial properties for SiC-based electronic devices. An increasing height of $Z_{1/2}$ with He fluence (Figure 5) is an evidence of $Z_{1/2}$ defect formation even in the cases with no annealing performed after implantation.

The $Z_{1/2}$ related DLTS peak in our non-thermally treated *as-implanted* 4H-SiC samples appears to be a broader than a typical peak for point-like defects. The asymmetry and the low-temperature shoulder

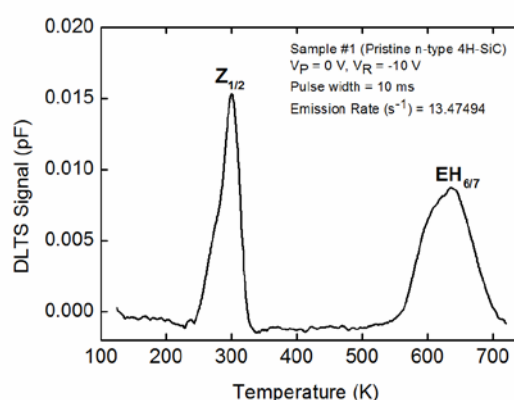


Figure 4. DLTS spectra of the pristine (#1) SBD sample measured at the maximum reverse bias voltage of -10 V, the filling pulse of $0V$, the pulse width of 10 ms and emission rate of 13.47 s⁻¹.

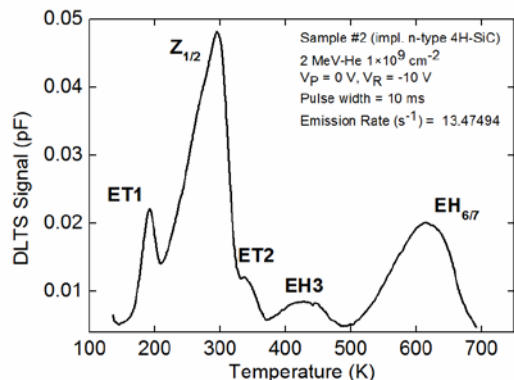


Figure 5. DLTS spectra obtained for the sample implanted with He ions (#2) for the reverse bias of -10 V, the filling pulse of 0 V, the pulse width of 10 ms, and the emission rate of 13.47 s⁻¹. During this measurement, the sample was annealed up to 700K for the first time.

observed at $Z_{1/2}$ peak (Figure 4) clearly indicate that it is not a single point-like defect. The broadening was enhanced after implantation of the 2 MeV He up to fluence of 1×10^9 cm⁻² (sample #2, Figure 5). As C-V measurements have indicated, the carrier removal effect is increasing with the fluence value (Figure 3). The uniform doping as measured before the implantation was significantly changed after the implantation.

D. Defects closely spaced to $Z_{1/2}$

In order to investigate in more detail the observed N-dopant deactivation or compensation effect connected with the defect “hidden” under the $Z_{1/2}$ and other defects introduced with ion implantation, we focused on the low-temperature part of DLTS spectra where the $Z_{1/2}$, ET1 and ET2 defects were observed during the first temperature scan between 100 K and 380 K. Therefore, we repeated the DLTS scan only up to 380 K. Within this low temperature range, DLTS spectrum with peaks corresponding to $Z_{1/2}$, ET1 and ET2 defects remained unchanged for the repeated DLTS measurement in comparison to DLTS spectrum obtained during the first low temperature scan.

Table II. The energy position and the effective carrier capture cross section for all observed defects in He implanted n-type 4H-SiC.

Defect label	E_t (eV)	σ (cm ⁻²)	Attribution
ET1 ^a	0.35	1×10^{-16}	Unknown
$Z_{1/2}$	0.64	3×10^{-15}	Vc(=0)
ET2 ^b	0.65	9×10^{-17}	Intrinsic
EH3 ^c	1.06	4×10^{-14}	Intrinsic
EH _{6/7}	1.84	1×10^{-12}	V _c (0/+)

^aEH1 in Ref.16, S1 in Refs. 36, 37, and S2 in Ref.35.

^bEH3 in Ref.16, S2 in Refs. 36, 37, S4 in Ref.35.

^cEH5 in Ref.16, S5 in Ref.35, ON2 in Ref.40, and RD1/2 in Ref.38.

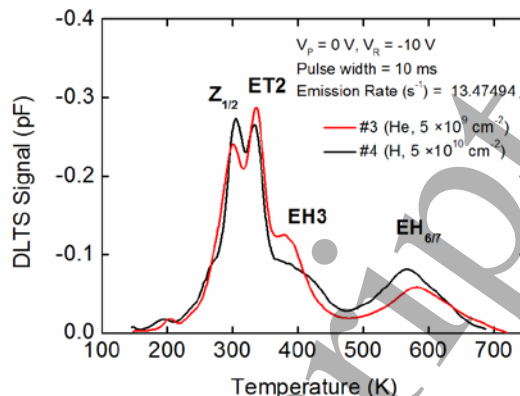


Figure 6. DLTS spectra obtained for samples implanted with He ions (#3) and H ions (#4), for the reverse bias of -10 V, the filling pulse of 0 V, the pulse width of 10 ms, and the emission rate of 13.47 s⁻¹. The spectra are recorded during the annealing to 700K for the first time.

Figure 6 shows DLTS spectra for samples implanted with 2.0 MeV He (#3) and 600 keV H ions (#4). The spectra were recorded during the first temperature scan up to 700K. The low-temperature part is identical as it was during the first and repeated measurements up to 380K, and we present this one in order to cover the full DLTS spectrum. As the He ion fluence increased, we clearly observed the peak closely spaced to the $Z_{1/2}$ peak, which we labelled as ET2. ET2 was a high-temperature shoulder, observed also in the sample implanted with the lowest ion fluence value (#2), Figure 5. To our best knowledge, such a strong increase in ET2 concentration compared to $Z_{1/2}$ concentration with the fluence, using the standard DLTS set-up and without any post implantation treatment, has not yet been observed or reported in literature. The activation energy for the ET2 was estimated to be 0.65 eV (Table II). The concentration of $Z_{1/2}$ in He implanted sample (#3) reached the value of $\sim 2 \times 10^{13}$ cm⁻³.

Parameters for all distinguished deep level defects that were created in He or H implanted n-type 4H-SiC epitaxial layers are summarized in Table II. The effective carrier capture cross sections were determined from the intercept of Arrhenius plots. In this study, we used the low N-doped 4H-SiC ($\sim 5 \times 10^{14}$ cm⁻³), and therefore we could not increase the fluence any further to obtain more reliable DLTS data. The ion implantation introduces many point like defects, acceptor like defects, which tend to react with positively ionized N creating several deep level defects according to compensation model [29, 30]. While the net free carrier concentration is decreasing with the fluence (C-V measurements; Figure 3), the concentration of defects created by ion implantation (such as ET2) is increasing (DLTS measurements; Figures 5 and 6). The concentration will reach saturation depending on the available nitrogen. The self-annealing of stable defects formed in each ion cascade, well separated in

2nd_revision_manuscript_JPCM-109666

space and time, assisted by successive randomly propagated projectiles in material, even before moving the fast raster-scanning microbeam to a new position, is reasonably to be assumed negligible in the *single ion regime* using the characteristic duration time of a thermal spike in the model developed by Seitz [31]. Assuming the zero recombination / annihilation of produced Frenkel pairs in initial ion cascades, the highest total concentration of vacancies or interstitials in narrow region of interest at depth of ~ 4600 nm in implanted samples #2 and #3 is approximately three times ($1.5 \times 10^{15} \text{ cm}^{-3}$) or more than one order of magnitude higher ($7.8 \times 10^{15} \text{ cm}^{-3}$) compared to the initial doping (or nitrogen) concentration ($5.1 \times 10^{14} \text{ cm}^{-3}$) in the pristine epitaxial 4H-SiC material (Figure 3). By overlapping the bias dependent $1/C^2$ profiles (symbols) with the calculated concentration profiles of carbon vacancies or interstitials given as a function of applied bias (lines), we estimated their concentration threshold value required for the carrier removal in our material to be approximately in the range of the nitrogen donor concentration of $5 \times 10^{14} \text{ cm}^{-3}$. This value is consistent with an observation of a very small change in the net free carrier concentration calculated from C-V measurements performed on the sample #2, that was implanted with the lowest He ion fluence ($1 \times 10^9 \text{ cm}^{-2}$) resulting with the highest total vacancy and interstitial concentration of approximately $1.5 \times 10^{15} \text{ cm}^{-3}$.

In order to check the origin of introduced defects, we implanted one SBD sample from the same batch with 600 keV H ions up to the fluence of $5 \times 10^{10} \text{ cm}^{-2}$ (#4). This fluence value was chosen on basis of the theoretical calculations of NIEL value scaling [32] for 600 keV H and 2 MeV He ions in silicon carbide using the SRIM outputs; $\sim 10^{-1} \text{ MeVcm}^2/\text{g}$ for the H ions compared to $\sim 10^0 \text{ MeVcm}^2/\text{g}$ for He ions. The total carbon vacancy or interstitial concentration reaches $\sim 6.3 \times 10^{15} \text{ cm}^{-3}$ at depth of ~ 4900 nm for the sample #4 implanted by 600 keV H which is above the threshold value deduced from C-V measurements performed on samples #2 and #3 implanted with He ions (Figure 3). Note that the calculated depth of maximum vacancy concentration in sample implanted with H ions (#4) matches the calculated depletion depth for bias of -10 V (Figure 3, cyan curve). Although a small fraction of vacancies was produced beyond the depletion region, the same deep level defects were created within tested depth with H ions as they were with He ions (Figure 6). Although the ratio of intensities of dominant $Z_{1/2}$ and ET2 defects is slightly modified, this result indicates the same origin of $Z_{1/2}$ and ET2 defects. Both $Z_{1/2}$ and ET2 are ion beam induced defects, and they do not depend on ion species. Their concentration depends on the total NIEL value of impinging particles into material.

E. Low temperature annealing of deep level defects

We repeated the DLTS measurements two months after the first temperature scan and with no additional annealing in between two measurements in order to check the influence of low-temperature annealing on defects introduced to studied N-doped 4H-SiC material by ion implantation in *single ion regime*. Figure 7 shows DLTS spectra for samples #3 and #4 recorded after annealing up to 700K which occurred during the first temperature scan. The very low-temperature annealing such as 700K ($426.85 \text{ }^\circ\text{C}$) introduced significant changes to defect population in implanted material, although the calculated activation energies required for migration, and transformation of point defects in 4H-SiC are much higher [33]. All implantation-induced defects (ET1, ET2, and EH3) beside the isolated carbon vacancy ($Z_{1/2}$ and $\text{EH}_{6/7}$) were annealed almost completely. Moreover, the intensity of $Z_{1/2}$ increased, while the $\text{EH}_{6/7}$ shifted on the temperature scale. The observed annealing behaviour of the solely ion implantation induced defect ET2, which was clearly distinguished from $Z_{1/2}$ even in the *as-implanted* samples, suggest that it is the defect of very low thermal stability which is related to intrinsic defects created in ion cascades, interstitials and vacancies in both carbon and silicon sub lattices. It is not related to the implanted ion H or He. The low activation energy suggests its relation to the carbon interstitial or carbon split-interstitial [33], although taking into an account that the most probable final annealing product of ET2 is $Z_{1/2}$ or $\text{EH}_{6/7}$, it can be related also to the carbon vacancy.

We also repeated the C-V measurements following the same experimental procedure explained above in order to check how the observed transformation of deep defects promoted by low temperature annealing up to 700 K has affected the free carrier concentration. Figure 8 shows

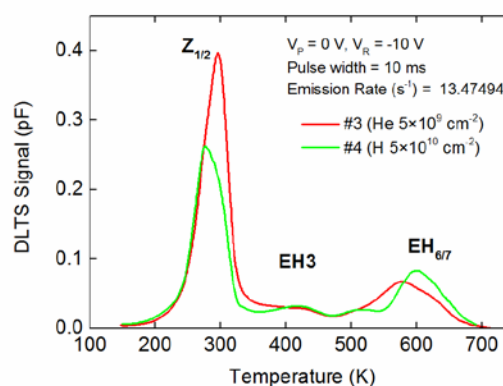


Figure 7. The repeated DLTS spectra recorded during the second temperature scan after the low temperature annealing of samples implanted with 2 MeV He (#3) and 600 keV (#4), for the reverse bias of -10 V, the filling pulse of 0 V, the pulse width of 10 ms, and the emission rate of 13.47 s^{-1} .

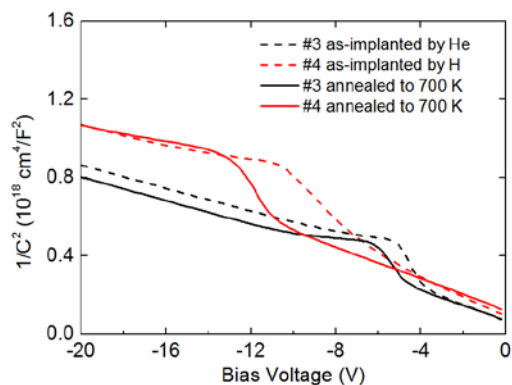


Figure 8. $1/C^2$ vs. V characteristics for the samples #3 and #4 before (dashed lines) and after (solid lines) low temperature annealing up to 700K.

combined results of the initial measurement on *as-implanted* samples (dashed lines) and of the repeated measurements on *as-annealed* samples (solid lines). It is clear that after low temperature annealing up to 700 K the free carrier concentration in both samples implanted with He (#3) and H (#4) increases in the region of interest. This recovery can be associated with transformation of the ion beam induced defects, in particular of the ET2 which is almost completely annealed out.

IV. DISCUSSION

The origin of ET1, ET2 and EH3 deep level defects is not clear. However, the ET1 and the high-temperature shoulder ET2 were already observed by Hemmingsson *et al.* in the low dose electron irradiated 4H-SiC samples [16]. Dalibor *et al.* have reported that in *n*-type 4H-SiC implanted with He ions, $Z_{1/2}$ -center related DLTS peak is overlapped by a second peak, which they were not able to resolve by their measurements [34]. Hemmingsson *et al.* have observed the same, and suggested that $Z_{1/2}$ (they have labelled it as EH2) peak consists of two overlapping components [16]. One of the components dominates for the low dose irradiation, and anneals out at 750 °C, while the other is stable at that temperature and it appears only after the high dose irradiation. Based on the dose dependency, annealing behaviour and similarity to the silicon vacancy in 3H and 6H-SiC, it was suggested that the low dose dominant peak is related to silicon vacancy [16]. Castaldini *et al.* have studied the low temperature annealing of electron irradiation induced defects in 4H-SiC [35]. Defects which they have labelled as S2, S2A and S3 resemble the low-temperature shoulder and the $Z_{1/2}$ defect observed in this study, respectively. They have proposed the two stage annealing process, the first one from 360 to 400 K, and the second from 400 to 700 K. During this stages, the S2A is decreasing, while S3 ($Z_{1/2}$)

is increasing and sharpening. It should be noted that DLTS peaks observed in their study are very broad and closely spaced which makes the direct comparison a little bit difficult. In their annealing study up to 100 °C Alfieri *et al.* observed formation of a deep level defect at 0.34 eV below E_C [36] known as S_1 [37], and transformation of the 0.60 eV peak revealing the presence of the $E_C-0.64$ level, labelled as $Z_{1/2}$ [16], and the so called S_2 level at $E_C-0.66$ eV in 15 MeV electron irradiated N-doped 4H-SiC [37]. Further annealing up to 200°C resulted in a shift of the S_1 , $Z_{1/2}$, and S_2 levels to deeper positions at 0.45, 0.70 and 0.72 eV below E_C . In the 12 MeV proton irradiated N-doped 4H-SiC which has been annealed at 100 °C for 20 min, the main very broad deep level with approximate energy at 0.62 eV below E_C is transformed in levels S_1 , $Z_{1/2}$, and S_2 as well [36]. The very broad EH3 peak could be EH4 and EH5, as reported by several authors [35, 38].

We have shown that the compensation of free charge carriers assigned to N-dopant deactivation is significant even for the low ion fluence value of 5×10^9 cm⁻² achieved using implantation in the *single ion regime*. Aberg *et al.* observed that the carrier removal is occurring at faster rate than the vacancy production in highly doped material [39]. Therefore they assigned carrier removal to N passivation through N-complex formation, and suggested the S_2 (or in our case the ET2) is N-related defect. They calculated activation energy for N-complex dissociation as 3.2 eV. We demonstrated that the initial concentration of carbon and silicon vacancies or interstitials (in the case of negligible annihilation) is comparable to the nitrogen concentration in samples where formation of the ET2 is clearly distinguished from the $Z_{1/2}$, so relation of the ET2 to substitutional nitrogen or carbon-nitrogen split-interstitials whose formation was predicted by Gertsman *et al.* [33] cannot be excluded. Further investigations are necessary to clarify the identity of ET1, ET2 and EH3 deep level defects investigated in this study.

V. CONCLUSIONS

To summarize, by using DLTS spectroscopy we distinguished presence and determined trapping parameters of several deep level defects which were formed in bulk N-doped 4H-SiC epi-layers following either H or He ion implantation in the *single ion regime* at room temperature with no additional thermal treatment of *as-implanted* samples. The first DLTS measurement revealed formation of deep level defects labelled as ET1 (0.35 eV), ET2 (0.65 eV) and EH3 (1.06 eV) which were clearly distinguished from the presence of dominant

2nd_revision_manuscript_JPCM-109666

carbon vacancies ($Z_{1/2}$ and $\text{EH}_{6/7}$) in increased concentrations after implantation of either H or He ions. We observed a particularly strong increase in ET_2 concentration compared to $Z_{1/2}$ concentration with the fluence, using the standard DLTS set-up and without any post implantation treatment, which has not yet been observed or reported in literature, in both cases of H and He ion implantation in the single ion regime. The second DLTS measurement revealed the almost complete removal of ET_2 and ET_1 defects, and the partial removal of EH_3 defect, while the concentrations of $Z_{1/2}$ and $\text{EH}_{6/7}$ defects were further increased, due to the relatively low temperature annealing up to 700 K, accomplished during the first temperature scan. It follows that the ET_2 and EH_3 deep level defects: i) act as majority carrier removal traps, ii) exhibit a low thermal stability and iii) can be related to the simple point-like defects introduced by light ion implantation, namely interstitials and/or complex of interstitials and vacancies in both carbon and silicon sublattices.

ACKNOWLEDGMENTS

This work is supported by the NATO SPS programme, project number 985215. The authors wish to acknowledge the National Collaborative Research Infrastructure Strategy (NCRIS) funding provided by the Australian Government for this research. The epitaxial films used in this study were grown by Central Research Institute of Electric Power Industry (CRIEPI). Authors would like to thank Dr N. Hoshino and Dr H. Tsuchida of the CRIEPI.

REFERENCES

- [1] L. M. Jong, J. Newnham, C. Yang, J. A. van Donkelaar, F. E. Hudson, A. S. Dzurak, and D. N. Jamieson, *Nucl. Instr. and Meth. Phys. Res.* 269, 2336 (2011).
- [2] J. C. McCallum, D. N. Jamieson, C. Yang, A. D. C. Alves, B. C. Johnson, T. F. Hopf, S. C. Thompson, J. A. Van Donkelaar, *Advances in Materials Science and Engineering* 2012, 272694 (2012).
- [3] A. D. C. Alves, J. Newnham, J. A. van Donkelaar, S. Rubanov, J. C. McCallum, D. N. Jamieson, *Nanotechnology* 24, 145304 (2013).
- [4] J. A. van Donkelaar, C. Yang, A. D. C. Alves, J. C. McCallum, C. R. Hougaard, B. C. Johnson, F. E. Hudson, A. S. Dzurak, A. Morello, D. Spemann, D. N. Jamieson, *J. Phys. Cond. Mat.* 27, 154204 (2015).
- [5] A. Dzurak, *Nature* 479, 47 (2011).
- [6] S. E. Saddow and A. K. Agarwal, *Advances in Silicon Carbide Processing and Applications* (Artech House, 2004).
- [7] P. G. Baranov, *JETP Lett.* 82, 441 (2005).
- [8] N. T. Son, P. Carlsson, J. Ul Hassan, E. Janzen, T. Umeda, J. Isoya, A. Gali, M. Bockstedte, N. Morishita, T. Ohshima, and H. Itoh, *Phys. Rev. Lett.* 96, 055501 (2006).
- [9] W. F. Koehl, B. B. Buckley, F. J. Heremans, G. Calusine and D. D. Awschalom, *Nature* 479, 84 (2011).
- [10] P. G. Baranov, A. P. Bundakova and A. A. Soltamov, *Phys. Rev. B* 83, 125203 (2011).
- [11] P. V. Klimov, A. L. Falk, B. B. Buckley and D. D. Awschalom, *Phys. Rev. Lett.* 112, 087601 (2014).
- [12] A. L. Falk, P. V. Klimov, B. B. Buckley, V. Ivády, I. A. Abrikosov, G. Calusine, W. F. Koehl, Á. Gali, D. D. Awschalom, *Phys. Rev. Lett.* 112, 187601 (2014).
- [13] S. Castelletto, B. C. Johnson, V. Ivády, N. Stavrias, T. Umeda, A. Gali, and T. Ohshima, *Nature Mater.* 13, 151 (2014).
- [14] H. J. von Bardeleben, J.-L. Cantin, E. Rauls, and U. Gerstmann, *Phys. Rev. B* 92, 064104 (2015).
- [15] S. A. Zargaleh, B. Eble, S. Hameau, J.-L. Cantin, L. Legrand, M. Bernard, F. Margaillan, J.-S. Lauret, J.-F. Roch, H. J. Von Bardeleben, E. Rauls, U. Gerstmann, and F. Treussart, *Phys. Rev. B* 94, 060102(R) (2016).
- [16] C. Hemmingsson, N. T. Son, O. Kordina, J. P. Bergman, E. Janzén, J. L. Lindström, S. Savage and N. Nordell, *J. Appl. Phys.* 81, 6155 (1997).
- [17] K. Danno, D. Nakamura, and T. Kimoto, *Appl. Phys. Lett.* 90, 202109 (2007).
- [18] N. T. Son, X. T. Trinh, L. S. Løvlie, B. G. Svensson, K. Kawahara, J. Suda, T. Kimoto, T. Umeda, J. Isoya, T. Makino, T. Ohshima, and E. Janzén, *Phys. Rev. Lett.* 109, 187603 (2012).
- [19] M. Ito, L. Storasta, and H. Tsuchida, *Appl. Phys. Express.* 1, 015001(3) (2008).
- [20] M.B.H. Breese, E. Vittone, G. Vizkelethy, P.J. Sellin, *Nucl. Instr. Meth. Phys. Res. B* 264, 345(2007).
- [21] E. Vittone, Z. Pastuovic, P. Olivero, C. Manfredotti, M. Jaksic, A. Lo Giudice, F. Fizzotti, E. Colombo, *Nucl. Instr. Meth. Phys. Res. B* 266, 1312 (2008).
- [22] Z. Pastuovic, R. Siegele, D. D. Cohen, M. Mann, M. Ionescu, D. Button, S. Long, *Nucl. Instr. Meth. Phys. Res. B* 404, 1 (2017).
- [23] M.B.H. Breese, G.W. Grime, F. Watt, *Annu. Rev. Nucl. Particle Sci.* 42, 1 (1992).
- [24] Ž. Pastuović, I. Capan, D.D. Cohen, J. Forneris, N. Iwamoto, T. Ohshima, R. Siegele, N. Hoshino and H. Tsuchida, *Nucl. Instr. and Meth. Phys. Res. B* 348, 233 (2015).
- [25] SRIM13: <http://www.srim.org>.
- [26] F. Nava, G. Bertuccio, A. Cavallini, E. Vittone, *Mat. Sci. Technol.* 19, 102001 (2008).
- [27] L.C. Kimerling, *J. Appl. Phys.* 45, 1839 (1974).
- [28] L. S. Løvlie and B. G. Svensson, *Appl. Phys. Lett.* 98, 052108 (2011).
- [29] A. Hallén, A. Henry, P. Pellegrino, B. G. Svensson, D. Aberg, *Materials Science and Engineering B* 61-62, 378 (1999).
- [30] D. Aberg, A. Hallén and B. G. Svensson, *Physica B* 273-274, 672 (1999).
- [31] F. Seitz, *Rev. Mod. Phys.* 26, 7 (1954).
- [32] S. R. Messenger, E. A. Burke, M. A. Xapsos, G. P. Summers, R. J. Walters, I. Jun and T. Jordan, *IEEE Trans. Nucl. Sci.* 50, 1919 (2003).
- [33] U. Gerstmann, E. Rauls, Th. Frauenheim, and H. Overhof, *Phys. Rev. B* 67, 205202 (2003).
- [34] T. Dalibor, G. Pensl, T. Kimoto, H. Matsunami, S. Sridhara, R. P. Devaty and W.J. Choyke, *Diamond and Related Materials* 6, 1333 (1997).
- [35] A. Castaldini, A. Cavallini, L. Rigutti, F. Nava, S. Ferrero and F. Giorgis, *J. Appl. Phys.* 98, 053706 (2005).
- [36] G. Alfieri, E.V. Monakhov, B.G. Svensson, M.K. Linnarsson, *J. Appl. Phys.* 98, 043518 (2005).
- [37] M. L. David, G. Alfieri, E. V. Monakhov, A. Hallen, C. Blanchard, B. G. Svensson, and J. Bardot, *J. Appl. Phys.* 95, 4728 (2004).
- [38] T. Dalibor, G. Pensl, H. Matsunami, T. Kimoto, W. J. Choyke, A. Schöner, N. Nordell, *Phys Status Solidi A* 162, 199 (1997).
- [39] D. Aberg, A. Hallén, P. Pellegrino and B.G. Svensson, *Appl. Phys. Lett.* 78, 2908 (2001).
- [40] H. M. Ayedh, V. Bobal, R. Nipoti, A. Hallén, B. G. Svensson, *Materials Science Forum* 858, 331 (2016).

1
2
3
4
5
6
7
8
9
10
11
12
13
14
15
16
17
18
19
20
21
22
23
24
25
26
27
28
29
30
31
32
33
34
35
36
37
38
39
40
41
42
43
44
45
46
47
48
49
50
51
52
53
54
55
56
57
58
59
60

Accepted Manuscript